Arch. Metall. Mater. **69** (2024), 3, 1191-1198

DOI: https://doi.org/10.24425/amm.2024.150942

A.I. ANUAR[1], N. PARIMIN[1,2*], N.A. AHAD[1,2], M.N. DERMAN[3], S. GARUS[4], P. VIZUREANU[5]

HIGH TEMPERATURE ISOTHERMAL OXIDATION AT 950°C OF Ni-BASED Fe-40Ni-24Cr ALLOY

The effect of different heat treatment temperatures on the isothermal oxidation of Ni-based Fe-40Ni-24Cr alloy was studied. The alloy underwent a heat treatment process at 1000°C and 1200°C for 3 hours of soaking time, followed by water quenching. These samples are labeled as N10 and N12. The heat-treated samples were characterized in terms of grain size using an optical microscope and hardness testing using a Rockwell hardness. As a result, increasing the heat treatment temperature increases the average grain size of the alloy and lowers the hardness value. Heat-treated N10 and N12 samples were subjected to an isothermal oxidation test at 950°C for an exposure time of 150 h. Oxidized heat-treated samples were characterized in terms of oxidation kinetics calculated based on weight change per surface area as a function of time. In addition, phase analysis and oxide surface morphology were measured using x-ray diffraction (XRD) and scanning electron microscopy (SEM) techniques. As a result, the oxidation kinetics of both samples showed a pattern of weight gain with N10 recording the lowest weight gain. Both samples obey a parabolic rate law, indicating a controlled oxide growth rate. N10 recorded the lowest parabolic rate constant of 2.5×10^{-8} $mg^2cm^{-4}s^{-1}$, indicating a low oxidation rate, thus having good oxidation resistance. Phase analysis using XRD shows that several oxide phases have been formed consisting of Cr-containing oxides Cr_2O_3 and $MnCr_2O_4$. In addition, SEM analysis displayed a uniform oxide layer formed on the N10 sample, indicating good oxide adhesion. This finding shows an important contribution to the oxidation protection mechanism that records the fine grain obtained from the heat treatment process can increase good oxidation resistance.

Keyword: Ni-based Fe-Ni-Cr alloys; Haynes HR-120 alloys; isothermal oxidation; heat treatment; oxidation kinetics

1. Introduction

Ni-based alloys are high-strength high-temperature alloys that have been modified to resist corrosion, oxidation and high temperature conditions [1]. The oxidation resistance of the alloys depends on the protective properties of the oxide layer formed on it surface in an oxidizing atmosphere [2]. Ni-based alloys are also used as materials for extreme environments and high temperature applications due to their superior high temperature mechanical properties [3], such as aircraft parts [4], turbine blades, turbine disks [5] and turbine engines [6]. This alloy has been widely used in energy and power applications due to its high temperature strength, high thermal stability, high corrosion resistance and good thermal fatigue resistance [7].

Ni-based alloys have increased strength and creep where these alloys will produce stable challenging phases such as precipitated carbides or intermetallic compounds [8]. In Ni-based alloys, there is the presence of Cr which can make the metal resistant to oxidation and can provide strength. Sufficient Cr content will increase the formation of protective oxide scale containing Cr elements such as Cr_2O_3 [2]. These Cr-containing oxides contribute to excellent oxidation resistance due to their protective behavior. On the other hand, other alloying elements are also added to the alloy system to improve specific properties depending on the desired goods [9].

Alloying elements such as Mn [2,10], Nb [11-12] and Ti [13] are usually added to NI-based alloy systems as carbide forming agents or precipitates due to their stable form. The addition of a small amount of Mn has contributed to the formation of a protective oxide layer consisting of a $MnCr_2O_4$ spinel structure [2]. Ti elements will also contribute to the formation of (Ti,Cr) O_2 fluorite oxide structure. The formation of Ti oxide consists of TiO_2 which is endowed with high corrosion resistance properties due to the formation of an oxide layer on the surface [13].

[1] UNIVERSITI MALAYSIA PERLIS (UNIMAP), FACULTY OF CHEMICAL ENGINEERING & TECHNOLOGY, 02600 ARAU, PERLIS, MALAYISA
[2] UNIVERSITI MALAYSIA PERLIS (UNIMAP), FACULTY OF CHEMICAL ENGINEERING & TECHNOLOGY, SURFACE TECHNOLOGY SPECIAL INTEREST GROUP, 02600 ARAU, PERLIS, MALAYSIA
[3] UNIVERSITI MALAYSIA PERLIS (UNIMAP), FACULTY OF MECHANICAL ENGINEERING & TECHNOLOGY, 02600 ARAU, PERLIS, MALAYISA
[4] CZESTOCHOWA UNIVERSITY OF TECHNOLOGY, FACULTY OF MECHANICAL ENGINEERING AND COMPUTER SCIENCE, 42-201 CZĘSTOCHOWA, POLAND
[5] GHEORGHE ASACHI TECHNICAL UNIVERSITY OF IASI, FACULTY OF MATERIAL SCIENCE AND ENGINEERING, 41 D. MANGERON ST., 700050 IASI, ROMANIA

* Coressponding author: noraziana@unimap.edu.my

Meanwhile, the addition of Nb into the alloy system will increase the formation of precipitates containing Nb such as Nb carbide [11-12]. The addition of Nb elements in small amounts to the alloy system also increases the high temperature oxidation resistance and thermal stability [14].

In addition, Al and Si are usually added to the Ni-based alloy system to increase oxidation protection by developing Al and Si oxide layers underneath the outer oxide layer. These oxides containing Al and Si elements will penetrate the base metal and form an internal oxide precipitate [15]. On the other hand, Al alloying elements also increase surface stability through the formation of Al_2O_3 oxide, contributing to good strength, good corrosion and good oxidation resistance. Other researchers also reported that the addition of Al and Si will affect the magnetic and mechanical properties of FeNiCo alloys [16].

In this study, a Ni-based Fe-40Ni-24Cr alloy was used, also known as Haynes HR-120 alloy, which is a heat-resistant solid solution alloy. The main characteristics of this alloy is its resistance to oxidation and carburizing conditions and also has high thermal strength [17]. Bar frames, heat treating baskets, radiant tubes, wire mesh furnace belts, and basket liners are examples of applications that demand high strength combined with strong resistance to high temperature oxidizing conditions. During high temperature exposure, oxide scale has developed on the surface of the alloy which acts as a protective layer to separate the alloy from the environment, thus protecting the component.

However, during high temperature exposure and prolonged service conditions, the occurrence of oxide spallation becomes a problem that reduces the protective behavior of the alloy surface. Reducing the oxide scale thickness on the alloy surface due to oxide exfoliation will expose the alloy to further oxidation damage. In order to overcome the peeling of oxides during prolonged heating, general studies have been carried out related to the heat treatment process to reduce the problem [18-19]. The fine grain size of the alloy has been recorded as an excellent oxidation protector to prevent oxide spallation [1,19-20].

One possible method to obtain fine grain size is by heat treatment process [21-22]. Therefore, in this study, the Ni-based Fe-40Ni-24Cr alloy underwent a series of heat treatment processes at different temperatures to change the grain size of the alloy. The fine and coarse grain size alloys obtained from the heat treatment process were subjected to isothermal oxidation tests to further analyze the effect of different grain sizes from the heat treatment process on the oxidation behavior of the Ni-based Fe-40Ni-24Cr alloy. Different grain size of Fe-40Ni-24Cr alloy obtained from the heat treatmenr process can provide beneficial findings ro examine the suitability of the optimum grain size to intensify good oxidation protection.

2. Materials and Methods

The Ni-based alloy consisting of Fe-40Ni-24Cr alloy used in this study, is a commercial Haynes HR-120 alloy (ASTM-B-409; ASME-SB-409, UNS N08120).The nominal chemical composition was measured using an optical emission spectrometer model Bruker Q8 MAGELLAN presented in TABLE 1. The sample dimensions are 10 mm×10 mm×3 mm.

TABLE 1

Chemical Composition of Ni-based Fe-40Ni-24Cr Alloy

Element	Content (wt%)
Ni	40
Cr	24
Mn	0.70
Si	0.44
Al	0.08
C	0.05
Nb	0.44
Ti	0.03
Mo	0.25
Co	0.17
Fe	Balance

The heat treatment process is carried out at two different temperatures of 1000°C and 1200°C, soaked for 3 hours, and then finished with rapid cooling in water. High temperature chamber furnace model SIC4-16LT was used for the heat treatment process. These samples are labeled as N10 and N12, respectively. The heat-treated samples were characterized in terms of grain size according to the ASTM E112 linear intercept method and the Rockwell hardness test. The microstructure of heat-treated sample for grain size measurement was examined using optical microscope model NIKON equipped with *i*-Solution image analysis software. Whereas, Digital Rockwell X series was used to measure the hardness. For the purpose of characterizing heat-treated samples, 5 samples were used for each temperature.Heat-treated N10 and N12 samples were subjected to isothermal oxidation at 950°C for 150 hours of exposure period.The furnace used for the isothermal oxidation test is a CARBOLITE tube furnace type 3HA 12/300 system. All samples were weighed on a METLER AT400 analytical balance with an accuracy of ±0.1 mg, before and after the oxidation test to measure weight change. Dimensions are measured by Mitutoyo Absolute Digimatic Caliper model CD-6“ CSX (±0.01 mm) in 12 locations. Average thickness and surface area values are calculated. In addition, all samples were ground to a P600 grit surface. To calculate oxidation kinetics, oxidation tests were conducted at 30-hour intervals for weight change measurements. For the purpose of determining the oxidation kinetics, 5 samples were used for each time interval of 30 h, with a total of 25 samples for each parameter. Oxidized samples were characterized in terms of phase analysis using the x-ray diffraction (XRD) technique model BRUKER D5000 XRD instrument software and surface morphology using a scanning electron microscope (SEM) equipped with energy dispersive x-ray (EDX) spectroscopy model JEOL JSM-6460 LA. The phase analysis was accomplished with the aid of DiffracPlus Evaluation Software and PDF-2 search/match applications to identify the phases of the oxide scales.

3. Results and Discussion

3.1. Heat treatment

Optical micrographs of samples N10 and N12 are shown in Fig. 1. The image shows the formation of grain structures with different sizes. The average grain size shows an increasing size as the heat treatment temperature increases. The heat-treated N10 sample recorded a fine grain structure of 27.17 µm, while the heat-treated N12 sample recorded a coarse grain structure of 49.56 µm. The hardness value is inversely proportional to the grain size, that is, when the heat treatment temperature increases, the hardness value decreases. Samples N10 and N12 recorded hardness values of 91.3 HRB and 87.5 HRB respectively. This finding is in line with previous studies, showing that when the heat treatment temperature increases, the grain size of the alloy will increase and the hardness will decrease [21]. The increase in grain size and decrease in the pattern of hardness value is also similar to the findings of other researchers, which is a study on solution treatment of Fe-Ni based alloys [22]. From these results, it shows that temperature is one of the contributing factors to control alloy grain growth.

3.2. Oxidation Kinetics

The oxidation kinetics of samples N10 and N12 after isothermal exposure at 150 hours is illustrated in Fig. 2. As a result, the alloy recorded a pattern of weight gain with the fine-grained N10 samples showing lower weight gain compared to coarse-grained N12 sample. The weight changes of both N10 and N12 followed the same trend with increasing exposure period. Both samples were quickly oxidized at an early stage. Then, the oxidation of N10 gradually turn into a steady increase in weight where the mass increases slowly. This observation is similar to the findings of other researchers, showing an increase in weight change as the duration of exposure increases gradually reaching a steady level [1,19]. On the other hand, the coarse-grained N12 sample recorded a steady increase in weight as the exposure period increased indicating that a thick oxide layer formed on the surface of the alloy. The weight gain trend is further analyzed according to equation (1) to determine the oxidation rate law of each sample.

The oxidation rate law was found using a double log plot, as shown in Fig. 3. The data were fitted using equation (1), where x is the weight change per surface area, t is time, and c

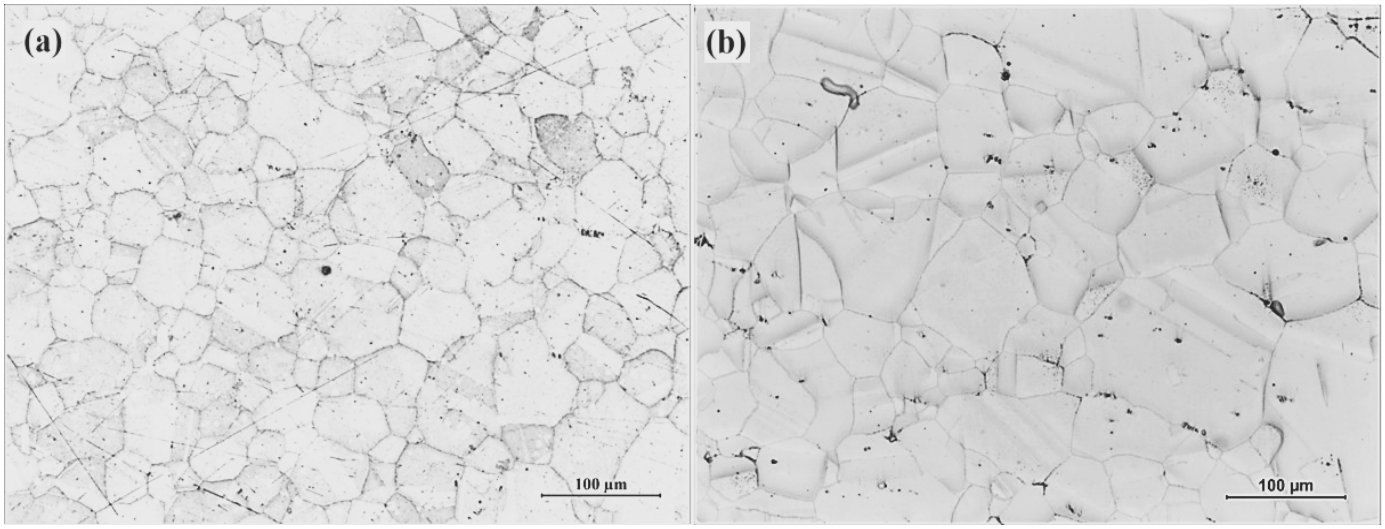

Fig. 1. Optical micrograph of N10 and N12

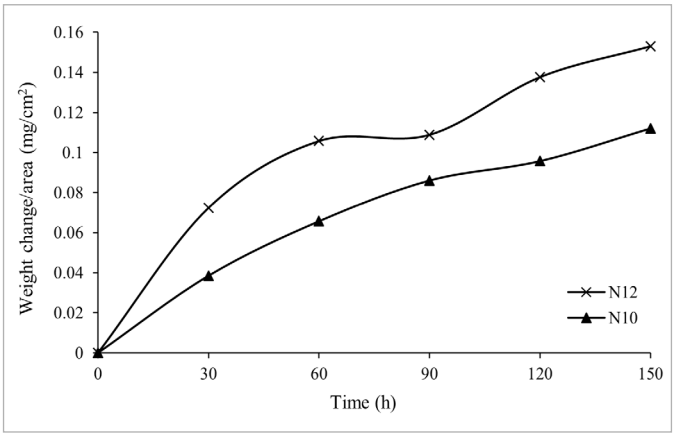

Fig. 2. Plot of weight change with time

and m are constants. Linear and parabolic oxidation rate laws are represented by values of m with 1, and 2, respectively, in a double log graphs. With m ranging from 1.50 to 2.49, which means a parabolic rate law (m = 2), both sample were fitted to this rate law recording m value of 2.24 and 1.52 for samples N10 and N12, respectively. All samples provided generally well-fitting findings. The values for the fitting parameter R^2 for N10 and N12 are 0.99, and 0.96, respectively. The R^2 value approaching one indicates that the data and fitting are becoming more consistent. Due to the alloy‘s superior influence on the rate of oxide formation, the parabolic rate law is preferred in this investigation. Oxide growth rate and sample weight gain for both samples are proportional to the parabolic rate law. Rapis initial oxide scale growth to coat the surface and further protect

the alloy causes the weight gain to jump significantly at the start of exposure. Then, as the exposure period increases due to the increase in oxide scale thickness, the rate of weight gain begins to slow. These findings indicate that the rate of oxide formation is controlled by diffusion.

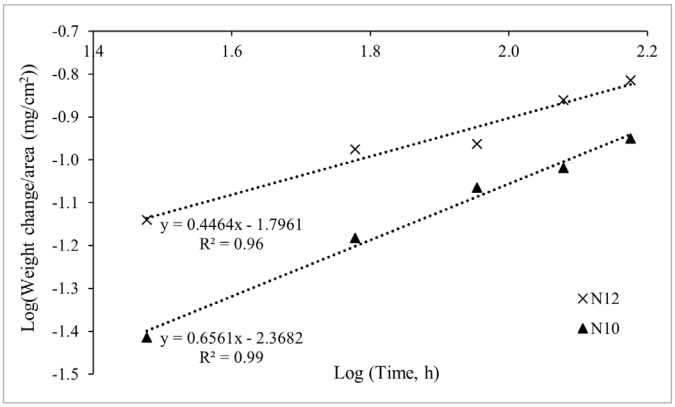

Fig. 3. Log plot of oxidation rate law analysis

The rate of diffusion-controlled oxide development is indicated by the oxidation kinetics of both samples, which follow a parabolic rate law. Diffusion of ionic species will gradually decrease as the oxide scale thickens, slowing the rate of oxidation. The oxidation kinetics of the fine-grained N10 sample showed a moderate oxidation rate with a consistent increase in weight as the duration of exposure increased.

Equation (2) is the parabolic rate law, used to obtain the parabolic rate constant, where *Kp* stands for the parabolic rate constant, *x* is the weight change per surface area, and *t* is the time in seconds. Fig. 4 displays a square plot of weight change per unit surface area as a function of time. Samples N10 and N12 all gave good results for the fitting parameters, with values of 0.99, and 0.96 for each sample, respectively. For samples N10 and N12, the parabolic rate constant, Kp, has values of 2.50×10^{-8} $mg^2cm^{-4}s^{-1}$, and 4.09×10^{-8} $mg^2cm^{-4}s^{-1}$ respectively. With a lower *Kp* value, the N10 sample shows a high oxidation resistance and a low oxidation rate. Since the fine-grained alloy has a larger grain boundary area, which serves as a diffusion channel for the upward migration of metal ions towards the metal surface, good

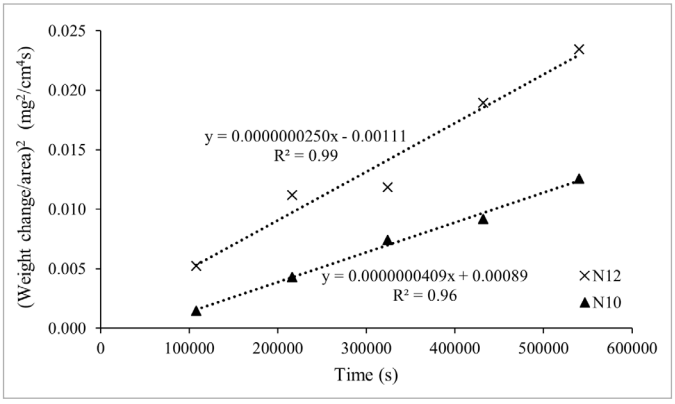

Fig. 4. Square plot of parabolic rate law analysis

oxidation resistance is obtained. This process results in the rapid production of an initial protective oxide layer that prevents the metal alloy from producing more oxide scale [19]. After a sufficient exposure period, an optimal oxide thickness forms on the surface, which provides adequate protection. After that, the oxidation rate starts to slow down, thus reducing the formation of the oxide layer, further stabelizing the weight gain, as shown in Fig. 1. This phenomenon is shown by the low value of the parabolic rate constant for this fine-grained N10 sample.

On the other hand, the coarse-grained N12 sample recorded a high parabolic rate constant value indicating a high oxidation rate. This result represents the higher weight gain recorded by this sample as shown in the oxidation kinetic curve in Fig. 1. The higher the oxidation rate, the higher the weight or scale of the oxide produced on the surface of the alloy.

$$\log x = 1/m \log t + c \quad (1)$$

$$x^2 = Kp\, t + c \quad (2)$$

3.3. X-ray diffraction analysis

Phase analysis using the XRD technique was performed for un-oxidized and oxidized samples at exposure periods of 30 and 150 hours. Both N10 and N12 samples show the same oxide formation on the alloy surface from XRD analysis. Sample N12 was further analyzed because this sample has a thicker oxide scale and more significant analysis can be done compared to sample N10. Fig. 5 shows phase analysis of un-oxidized sample N12 recorded a formation of main peak of Ni-based Fe-40Ni-24Cr alloy label as Fe-Ni-Cr. Three sharp peaks detected at 2θ 44.1°, 51.2° and 75.2°. Figs. 6 and 7 show the phase analysis of N12 samples at 30 and 150 hours to better understand the behavior of oxide scale formation. Due to the similar pattern between the two samples, this N12 sample was chosen to represent the phase analysis. From the peak analysis in Fig. 6, the base alloy labeled as Fe-Ni-Cr has the sharpest peak at 2θ 44.1°, then followed by other peaks at 51.2° and 75.2°. The higher intensity of the base alloy peak indicates that a thin oxide layer has formed on the surface. On the other hand, a protective oxides scale consisting of Cr_2O_3 and $MnCr_2O_4$ were also detected. This oxide phase records several multiple peaks at several 2θ due to the finite size of the oxide phase crystals. A comprehensive and extensive analysis was performed to identify the phases present, thus identifying these two peaks.

Fig. 7 shows the N12 sample after 150 hours of exposure. The oxides containing the most Cr are found to be Cr_2O_3 and $MnCr_2O_4$. Cr-containing oxides have protective oxide behavior. In addition, the incorporation of Mn elements into Cr oxide $MnCr_2O_4$ can reduce the influence of Cr_2O_3 evaporation [2,23]. On the other hand, base alloys with low intensity peaks are also detected labeled as Fe-Ni-Cr. This observation shows a thick oxide layer formed on the surface of the alloy after exposure for 150 hours. The formation of Cr_2O_3 and $MnCr_2O_4$ oxide phases is

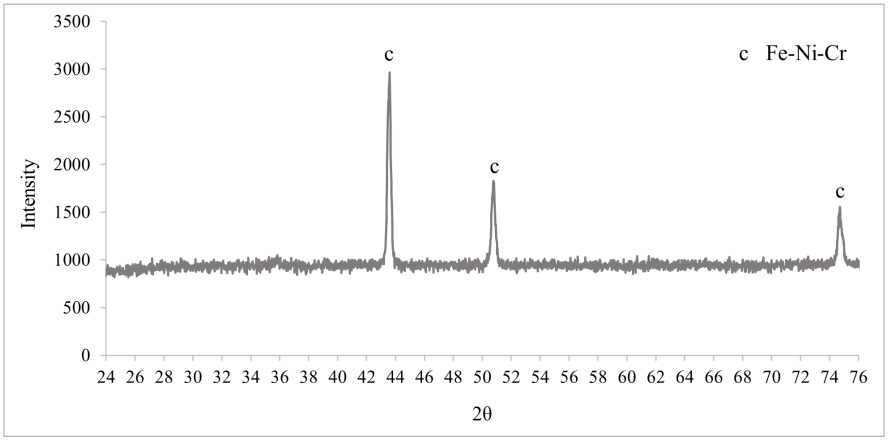

Fig. 5. XRD analysis of un-oxidized N12 sample

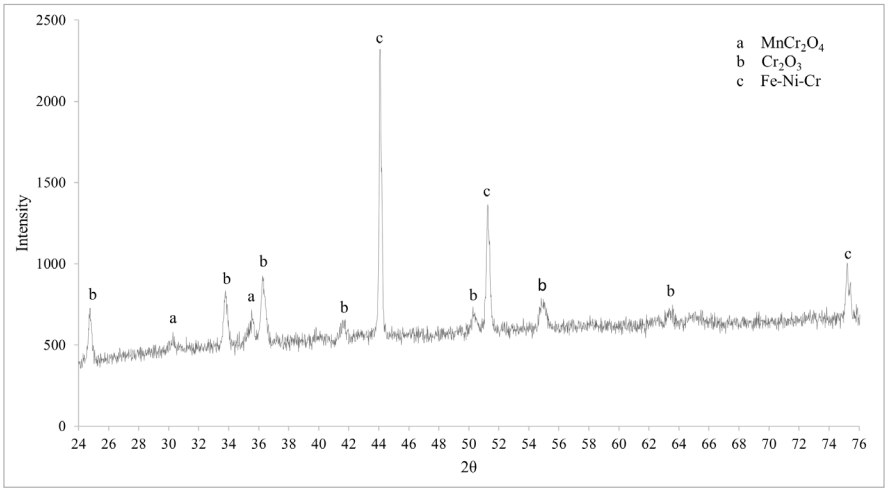

Fig. 6. XRD analysis of oxidized N12 sample after 30 h

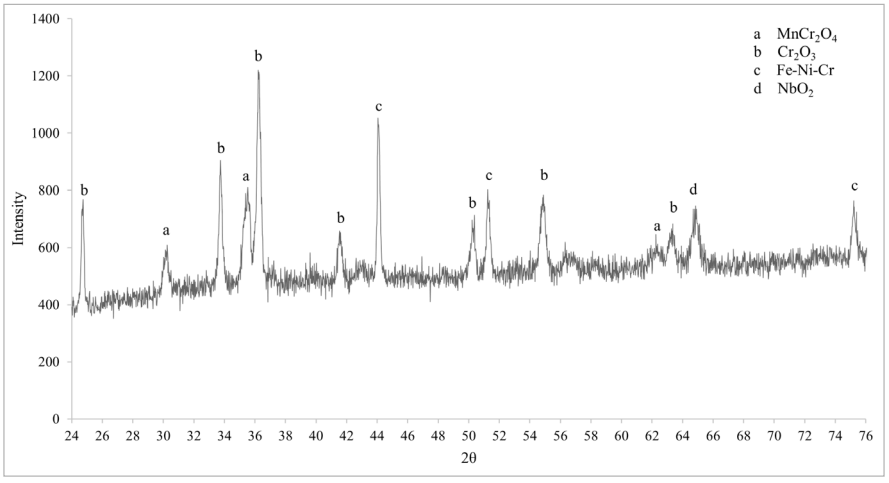

Fig. 7. XRD analysis of oxidized N12 sample after 150 h

desired in this study because of their protective behavior. These oxides have good adhesion to the base alloy which reduces the tendency of oxide spallation. The combination of Mn-Cr oxide has improved oxidation protection [2].

Phase analysis at 150 hours exposure also revealed the formation of NbO_2 oxide. The element Nb has been added to alloys to improve their properties, and contributes to the formation of precipitates and oxide phases [5,11-12]. However, this oxide is prone to give excessive growth which will contribute to the possibility of oxide spallation as reported in previous work [17]. The behavior of this oxide was further studied in SEM analysis.

3.4. Scanning electron microscope analysis

Analysis by scanning electron microscopy (SEM) was performed to identify the surface morphology of the oxide scale formed. Fig. 8 shows the SEM image of the N10 sample showing a continuous and uniform oxide layer formed on the surface of the alloy. However, there is a small area of oxide spallation that occurs as shown in the red line of the rounded rectangle shape in the image. Observations on this image show that the oxide spallation occurrence only peels off the outer layer of the oxide scale without exposing the base metal as shown on the left side of the label. This phenomenon is consistent with the oxidation kinetic curve of this sample which shows a stable increase of weight gain. The occurrence of oxide spallation on this sample did not cause the protective layer to be exposed, therefore it did not cause the formation of a fresh oxide layer to seal the unprotected area which would cause an increase in weight.

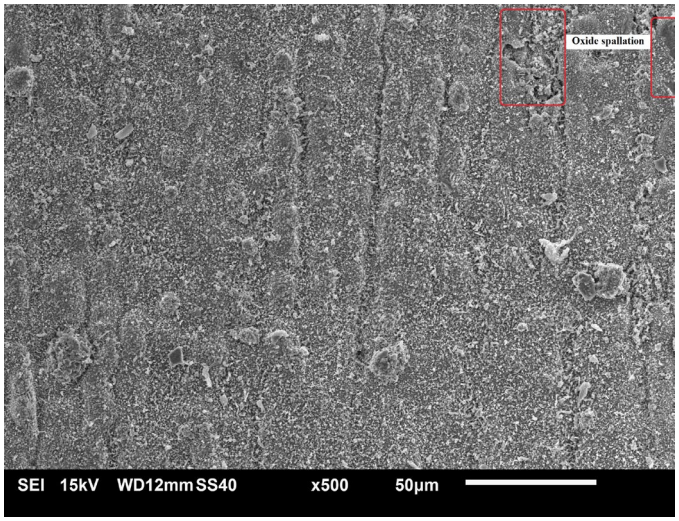

Fig. 8. SEM image of N10 sample

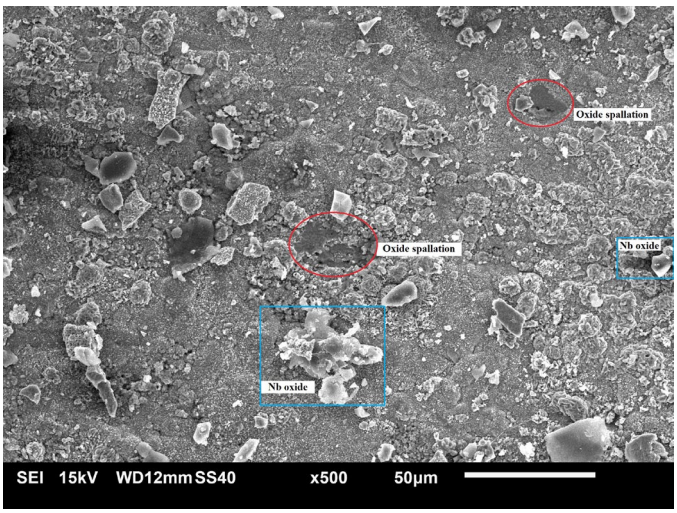

Fig. 9. SEM image of N12 sample

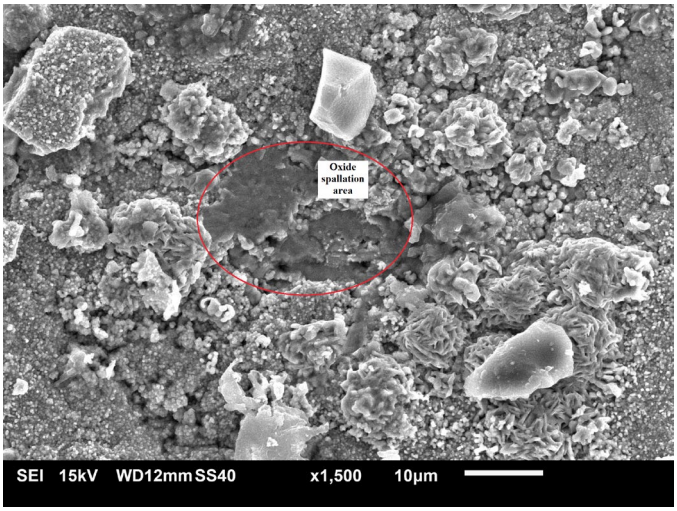

Fig. 10. SEM image of N12 sample in spallation area

On the other hand, Fig. 9 shows the SEM image of sample N12 showing the formation of oxide spallation in some areas shown in the red line of the oval shape with the addition of some growth of oxide particles on the surface shown in the blue line of the rectangle shape. Although there was oxide exfoliation on the N10 sample, this exfoliation did not cause severe damage compared to the N12 sample. Oxide exfoliation occurs on the N12 sample causing the generation of voids around the oxide spallation area as illustrated in Fig. 10 with a close-up view in the red line of the oval shape. Instead, there is evidence of loose oxide structures adjacent to spallation areas, these structures have a tendency to exfoliate causing other oxidation damage.

EDX analysis of the N12 sample on the particles in the rectangular blue line recorded the elements of Nb and O on the large-sized oxide particles, suggesting the formation of Nb oxide particles, as shown in Fig. 11. The NbO_2 oxide phase was detected through XRD analysis which proved the formation of this Nb oxide. As previously studied, the formation of Nb oxide particles has a tendency to have a higher growth rate that is prominent on the oxide surface area [17]. This mechanism will cause the generation of cracks around the excessively large Nb oxide particles, with prolonged exposure causing the oxide to come off leaving an unprotected area around the spallation area. As unprotected areas occur, fresh oxide will form to wrap around the unprotected areas causing an increase in oxide thickness. This phenomenon is consistent with the oxidation kinetics curve of this sample, showing a higher weight gain with a high parabolic rate constant. Higher parabolic rate constants reflect higher oxidation rates.

The addition of Nb elements into the Fe-40Ni-24Cr alloy is to improve its properties, but to a certain extent will cause the uncontrolled growth of Nb-rich oxides that cause oxide spallation. This phenomenon will be reduced by providing a fine-grained alloy structure. The fine grain structure has a diffusion-controlled oxide mechanism, which also has a lower oxidation rate, thus reducing the tendency of unwanted Nb oxide particle overgrowth.

Overall, this study shows significant findings on the oxidation resistance behavior of Ni-based fine grain Fe-40Ni-24Cr

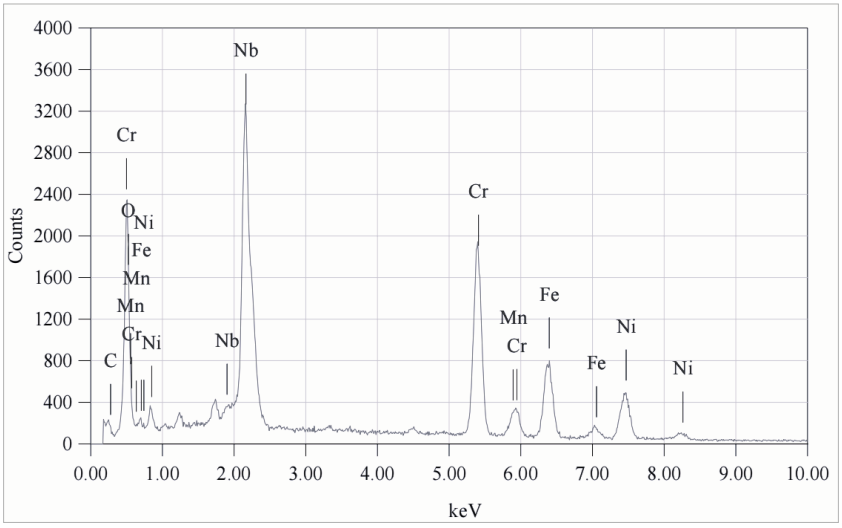

Fig. 11. EDX analysis of N12 sample

alloys. Further research is aimed at in-situ analysis and characterization of oxide formation on isothermal and cyclic oxidation tests to better understand the behavior of oxide scale formation.

4. Conclusions

Isothermal oxidation of Fe-40Ni-24Cr alloy was performed on fine-grained heat-treated N10 sample and coarse-grained heat-treated N12 sample and the important conclusions can be reported as follows:

i. The N10 sample exhibits a low parabolic rate constant indicating a low oxidation rate, thus having good oxidation resistance. In addition, the N10 sample displayed a uniform oxide scale formed on the surface of the alloy.
ii. In contrast, sample N12 exhibits a high parabolic rate constant indicating a high oxidation rate with evidence of some oxide spallation.

Acknowledgments

This research was funded by the Ministry of Higher Education Malaysia under the Fundamental Research Grant Scheme (FRGS) FRGS/1/2020/TK0/UNIMA)/02/43.

REFERENCES

[1] X. Wang, J.A. Szpunar, Effects of grains sizes on the oxidation behavior of Ni-based alloy 230 and N. Journal of Alloys and Compounds **752**, 40-52 (2018).
DOI: https://doi.org/10.1016/j.jallcom.2018.04.173

[2] T.D. Nguyen, J. Zhang, D.J. Young, Effect of Mn on oxide formation by Fe-Cr and Fe-Cr-Ni alloys in dry and wet CO2 gases at 650°C. Corrosion Science **112**, 110-127 (2016).
DOI: https://doi.org/10.1016/j.corsci.2016.07.014

[3] C.N. Athreya, K. Deepak, D.I. Kim, B. Boer, S. Mandal, V.S. Sarma, Role of grain boundary engineered microstructure on high temperature stream oxidation behavior of Ni based superalloy alloy 617. Journal of Alloys and Compounds **778**, 224-233 (2019).
DOI: https://doi.org/10.1016/j.jallcom.2018.11.137

[4] J. Jiang, G. Xiao, Y. Wang, Y. Liu, High temperature oxidation behavior of the wrought Ni-based superalloy GH4037 in the solid and semi-solid state. Journal of Alloys and Compounds **784**, 394-404 (2019).
DOI: https://doi.org/10.1016/j.jallcom.2019.01.093

[5] L. Jung-Uk, K. Young-Kyun, S. Seong-Moon, L. Kee-Ahn, High Temperature Oxidation Property of Ni Based Superalloy CM247LC Produced Via Selective Laser Melting Process. Arch. Metall. Mater. **68** (1), 107-112 (2023).
DOI: https://doi.org/10.24425/amm.2023.141481

[6] Z. Nanfu, W. Zheng, L. Yang, L. Xinghong, J. Tao, Columnar Dendrite Morphology and Solute Concentration of GH3039 Nickel-Based Superalloys during Wire and Laser Additive Manufacturing: Insights from Phase Field Simulations. Arch. Metall. Mater. **68** (1), 387-393 (2023).
DOI: https://doi.org/10.24425/amm.2023.143673

[7] S. Dodla, Experimental Investigation of Tool Wear in Vibration-Assisted Turning of Inconel 718. Arch. Metall. Mater. **67** (3), 949-953 (2022).
DOI: https://doi.org/10.24425/amm.2022.139687

[8] R.C. Reed, C.M.F. Rae, Physical Metallurgy of the Nickel-Based Superalloys. Physical Metallurgy (Fifth Edition), 2215-2290 (2014).
DOI: https://doi.org/10.1016/B978-0-444-53770-6.00022-8

[9] L. Sharma, S.K. Chaubey, To Study the Microstructural Evolution of EN353 Steel under Different Heat Treatment Conditions. Arch. Metall. Mater. **68** (2), 423-430 (2023).
DOI: https://doi.org/10.24425/amm.2023.142418

[10] G.R. Holcomb, D.E. Alman, The Effect of Manganese Additions on the Reactive Evaporation of Chromium in Ni-Cr Alloys, Scripta Materialia **54** (10), 1821-1825 (2006).
DOI: https://doi.org/10.1016/j.scriptamat.2006.01.026

[11] Y.X. Xu, J.T. Lu, W.Y. Li, X.W. Yang, Oxidation behavior of Nb-rich Ni-Cr-Fe alloys: Role and effect of carbides precipitates. Corrosion Science **140**, 252-259 (2018).
DOI: https://doi.org/10.1016/j.corsci.2018.05.040

[12] Y.X. Xu, J.T. Lu, X.W. Yang, J.B. Yan, W.Y. Li, Effect and role of alloyed Nb on the air oxidation behaviour of Ni-Cr-Fe alloys at 1000°C. Corrosion Science **127**, 10-20 (2017).
DOI: https://doi.org/10.1016/j.corsci.2017.08.003

[13] G. Dercz, I. Matula, K. Prusik, J. Zajac, M. Szklarska, A. Kazek-Kesik, W. Simka, Effect of Nb and Zr alloying additives on structure and properties of Ti-Ta-Nb-Zr alloys for medical applications. Arch. Metall. Mater. **68** (3), 1137-1142 (2023).
DOI: https://doi.org/10.24425/amm.2023.145485

[14] Y.H. Cho, G.S. Ham, S.Y. Park, C.P. Kim, K.A. Lee, Effect of Nb and Mo Addition on the Microstructure and Wear Behavior of Fe-Cr-B Based Metamorphic Alloy Coating Layer Manufactured by Plasma Spray Process. Arch. Metall. Mater. **67** (4), 1521-1524 (2022).
DOI: https://doi.org/10.24425/amm.2022.141086

[15] J. Zurek, D.J. Young, E. Essuman, M. Hänsel, H.J. Penkalla, L. Niewolak, W.J. Quadakkers, Growth and Adherence of Chromia Based Surface Scales on Ni-Base Alloys in High- and Low-pO2 Gases. Materials Science and Engineering: A **477** (1-2), 259-270 (2008).
DOI: https://doi.org/10.1016/j.msea.2007.05.035

[16] B. Kurowski, D. Oleszak, Influence of Aluminium ans Solicon Content on the Phase Composition, Microstructure and Magnetic and Mechanical Properties of Multicomponent FeNiCoAlSi Alloys. Arch. Metall. Mater. **68** (2), 765-768 (2023).
DOI: https://doi.org/10.24425/amm.2023.142459

[17] N. Parimin, E. Hamzah, Effect of Nb on Oxide Formation by Isothermal Oxidation of Solution Treated Fe-40Ni-24Cr Ni-Based Alloy. Solid State Phenomena **336**, 11-16 (2022).
DOI: https://doi.org/10.4028/p-2je8fv

[18] A. Munitz, S. Salhov, G. Guttmann, N. Derimow, M. Nahmany, Heat treatment influence on the microstructure and mechanical properties of AlCrFeNiTi0.5 high entropy alloys. Materials Science and Engineering A **742**, 1-14 (2019).
DOI: https://doi.org/10.1016/j.msea.2018.10.114

[19] N. Parimin, E. Hamzah, Oxidation Kinetics of Fe-Ni-Cr Alloy at 900ºC. Materials Science Forum **1010**, 58-64 (2020).
DOI: https://doi.org/10.4028/www.scientific.net/MSF.1010.58

[20] A. Munitz, L. Meshi, M.J. Kaufman, Heat treatments' effects on the microstructure and mechanical properties of an equiatomic Al-Cr-Fe-Mn-Ni high entropy alloy. Materials Science and Engineering A **689**, 384-394 (2017).
DOI: https://doi.org/10.1016/j.msea.2017.02.072

[21] N. Parimin, E. Hamzah, Influence of Solution Treatment Temperature on the Microstructure of Ni-based HR-120 Superalloy. IOP Conference Series: Materials Science and Engineering **957**, 012003 (2020).
DOI: https://doi.org/10.1088/1757-899X/957/1/012003

[22] J.F. Zhang, Y.F. Tu, J. Xu, J.S. Zhang, J.L. Zhang, Effect of Solid Solution Treatment on Microstructure of Fe-Ni Based High Strength Low Thermal Expansion Alloy. Journal of Iron and Steel Research, International **15** (1), 75-78 (2008).
DOI: https://doi.org/10.1016/S1006-706X(08)60016-3

[23] N. Parimin, E. Hamzah, Role of Mn Alloying Element on the Oxide Growth Behavior of 800H Nickel-Based Alloy at 900°C. Solid State Phenomena **336**, 17-22 (2022).
DOI: https://doi.org/10.4028/p-qel84v